



# Fibrillatory conduction in a simulated two-dimensional model of human atrial tissue: effect of the interaction of two ectopic foci

Catalina Tobón<sup>1</sup>  and Javier Saiz<sup>2</sup>

## Abstract

Atrial fibrillation (AF) is the most common tachyarrhythmia. It has been demonstrated that extra-stimuli could act as triggers for AF. In many patients it is possible that multiple ectopic foci co-exist, and their interactions may generate complex conduction patterns. Our goal is to investigate the influence of the focus frequency, conduction velocity, and anisotropy on fibrillatory pattern generation during the interaction of multiple ectopic activities under electrical remodeling conditions.

Our results support the broadly accepted theory that ectopic activity acting in remodeled tissue is an initiator of reentrant mechanisms. These reentrant circuits can generate fibrillatory activity when interacting with other rapid ectopic foci and under the following conditions: high ectopic focus frequency, slow conduction velocity, and anisotropic tissue. Analyses of electrogram polymorphism allow determination of which zones of tissue permit one to know in which zone of tissue unstable activity exists.

Our results give useful insights into the electrophysiological parameters that determine the initiation and maintenance of fibrillatory conduction by two ectopic foci interaction in a simulated two-dimensional sheet of human atrial cells, under chronic AF conditions.

## Keywords

Two-dimensional atrial model, fibrillatory conduction, ectopic activity

## 1. Background

Atrial fibrillation (AF) is the most common atrial tachyarrhythmia. The presence of AF is associated with a considerable increase in morbidity and mortality.<sup>1</sup> This arrhythmia remains one of the major causes of stroke, heart failure, and cardiovascular morbidity in the world.<sup>2–4</sup> The prevalence of AF is approximately 2% of the general population, double that reported in the last decade. AF is present in 0.12–0.16% of those younger than 49 years, in 3.7–4.2% of those aged 60–70 years, and in 10–17% of those aged 80 years or older.<sup>5,6</sup> The incidence of AF ranges between 0.21 and 0.41 per 1000 person/years.<sup>5</sup> Recent studies show that 20–30% of patients with stroke have AF diagnosed before, during, or after the initial event.<sup>7</sup> Cognitive damage<sup>8</sup> and decreased quality of life<sup>9</sup> are common in AF patients. Between 10% and 40% of AF patients are hospitalized each year.<sup>10</sup> The number of patients with AF is predicted to rise notably in the coming years.<sup>11</sup>

Although considerable advances in the treatment of AF have taken place, the results of the pharmacologic and surgical treatment are still suboptimal. This is due, mainly, to the lack of knowledge that still exists about the pathophysiological mechanisms that cause the initiation and maintenance of this arrhythmia. Rhythm control can be achieved by ablation therapy. The aim of ablation procedures for AF is the electrical isolation of pulmonary veins (PVs) from the left atrium. The rationale for this is the crucial observation by Haissaguerre et al.<sup>12</sup> that AF was almost always triggered by ectopic beats arising from the muscle sleeves of the PVs. They demonstrated that extra-stimulus

<sup>1</sup>MATBIOM, Universidad de Medellín, Colombia

<sup>2</sup>CI<sup>2</sup>B, Universitat Politècnica de Valencia, Spain

## Corresponding author:

Catalina Tobón, MATBIOM, Universidad de Medellín, Carrera 87 N° 30 - 65, Medellín, Colombia.

Email: ctobon@udem.edu.co

and atrial rapid paces originating in the interior or in the proximities of the PVs could act like triggers and, in some cases, they would be responsible for the maintenance of focal AF episodes.<sup>13,14</sup> Whereas paroxysmal AF is predominantly driven by focal activity or local reentry from one or more PVs, as the arrhythmia evolves toward more persistent forms promoted by the several types of atrial remodeling, AF-maintaining mechanisms move toward the atria and are increasingly based on reentry substrates.<sup>15–18</sup> Based on clinical<sup>19–21</sup> and experimental<sup>22,23</sup> results, certain types of AF can be attributed to stable high-frequency rotor waves whose periodic activation can be converted into a chaotic pattern when the wavefronts propagate across the atrial wall. This phenomenon, known as the mother rotor hypothesis, is the most recent proposed mechanism of AF.<sup>24</sup> Rotor waves have been shown in computer models of AF so far.<sup>25,26</sup>

Experimental studies have demonstrated that high-frequency ectopic activity contributes to the generation of fibrillatory conduction.<sup>19,22,27,28</sup> A single focal trigger may result in a rapid reentrant circuit or rotor maintained in the PVs, since a tight-coupled extra-stimulus within PVs or in their proximity can result in unidirectional conduction block and reentry.<sup>27,29</sup> Other functional regions, such as the left atrial free wall, superior vena cava, inferior vena cava, crista terminalis, coronary sinus, and interatrial septum, have also been found to play critical roles in the initiation of AF. Besides, in many patients it is possible that multiple ectopic foci co-exist,<sup>12,13,27,28,30,31</sup> and their interactions may generate complex atrial conduction patterns facilitating the development and maintenance of AF.

It is well known that atrial remodeling caused by rapid and irregular activation of the atrium during atrial arrhythmias induces electrical changes, causing the reduction in refractoriness provoked by a significant action potential duration (APD) shortening.<sup>15,32–35</sup> A unifying theory suggests that the rapid focal activity promotes atrial remodeling that is required to maintain a substrate capable of rotors and multiple wavelet reentries.<sup>36,37</sup>

Another factor that favors the development of AF is a slow conduction velocity. Experimental studies<sup>27,38,39</sup> have observed a marked decrease of the conduction velocity in the proximal region of the PVs, contributing to the generation of chaotic activity. It has also been demonstrated that the intrinsic anisotropy of the tissue favors the generation of wavebreak and fibrillatory conduction.<sup>40–42</sup>

Although the existence of both spontaneous and induce ectopic activity and the interaction of multiple foci have been amply demonstrated, is not clear how parameters such as the frequency of stimulation, conduction velocity, and anisotropy affect the fibrillatory patterns. Here we construct a biophysical computer model of electrical activity for two-dimensional (2D) human atrial tissue, including orifices for the right PVs. The model was used to study the influence of the interaction of multiple ectopic activities

on fibrillatory pattern generation under electrically remodeled atrial tissue. We analyzed the interaction between stable ectopic activity arising from the right atrium with a burst of ectopic beats firing in the right PVs, and we studied the effects when we modified the ectopic focus frequency, the conduction velocity, and the anisotropy of the atrial tissue on the generation of fibrillatory conduction.

## 2. Methods

### 2.1 Model description and implementation

The Nygren model<sup>43</sup> of human atrial action potential was implemented to reproduce cell electrical activity. This model consists of a Hodgkin–Huxley-type equivalent circuit for the sarcolemma, coupled with a fluid compartment model, which accounts for charges in ionic concentrations in the cytoplasm as well as in the sarcoplasmic reticulum.

To reproduce atrial remodeling, the changes in ionic channel conductance and kinetics of human atrial myocytes in experimental studies of AF, reported by Bosch et al.<sup>32</sup> and Workman et al.,<sup>33</sup> have been incorporated into the model of human action potential. Several parameters were changed: the channel conductance for  $I_{K1}$  was increased by 250%, for  $I_{CaL}$  it was decreased by 74%, and for  $I_{to}$  it was decreased by 85%; the kinetics of the fast inactivation of  $I_{CaL}$  was increased by 62%, the activation curve of  $I_{to}$  was shifted by + 16 mV, and the inactivation curve of  $I_{Na}$  was shifted by + 1.6 mV.

Differences in APD among physiological and remodeling models were computed from the 10th stimulus after pacing the models at a basic cycle length of 1 second. Changes in APD were noted. Figure 1(a) displays the simulated action potentials in a single atrial cell under physiological and remodeling conditions. Electrical remodeling causes a significant shortening of APD from 312 ms to 92 ms. The electrical remodeling also induces a 6 mV hyperpolarization of the resting potential.

Action potential restitution was computed applying a premature stimulus after the 10th stimulus of the pacing. The coupling interval (CI) was defined as the time interval between the upstroke of the previous action potential and the upstroke of the current action potential. A plot of APD against CI gave APD restitution, as shown in Figure 1(b). The effective refractory period (ERP) was defined as the minimum time interval between the 10th stimulus of the pacing and the premature stimulus that produced an action potential with peak potential over 80% of the last action potential peak potential. Electrical remodeling provokes ERP shortening from 284 to 86 ms.

The electrophysiological model was integrated in a 2D model of the human left atrial tissue including two orifices for right PVs (see Figure 2). The size of the atrial tissue was 9.6 cm × 9.6 cm, which was discretized by a spatial resolution of 0.24 mm to form a 400 × 400 node discrete

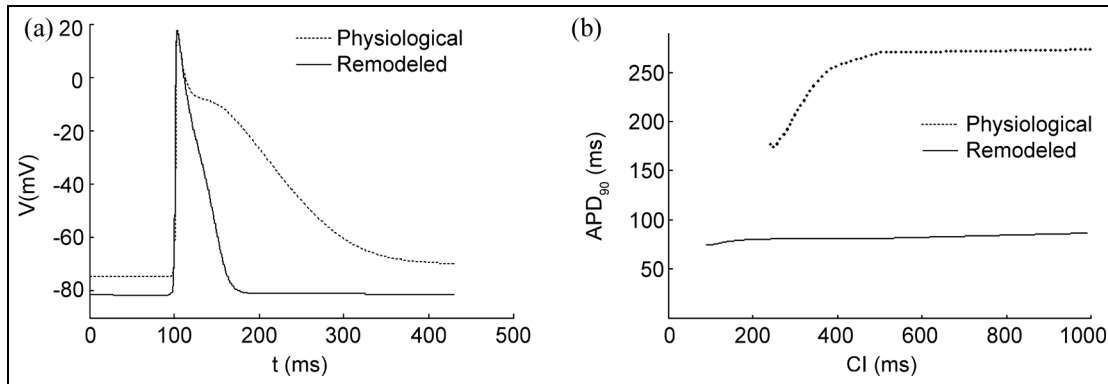


**Figure 1.** (a) Simulated action potentials and (b) electrical restitution plotted as action potential duration versus the coupling interval (Cl) in physiological and remodeling conditions.

lattice. These dimensions generate  $92 \text{ cm}^2$  of area, simulating half of the normal human left atrium.<sup>44</sup> Two circular regions of 1.1 cm diameter and null conductivity were added to simulate the orifices of the right PVs. The tissue includes part of the right-hand sidewall of the left atrium, where the Bachmann bundle (BB) ends; part of the superior wall, where the interatrial septum (IS) ends; and part of the free wall of the left atrium.

The propagation of action potential along the tissue model is described by the reaction-diffusion equation:

$$\frac{1}{S_v} \nabla(D \nabla V_m) = C_m \frac{\partial V_m}{\partial t} + I_{ion} - I_{st} \quad (1)$$

where  $S_v$  corresponds to the surface-to-volume ratio ( $2.5 \cdot 10^4 \text{ m}^{-1}$ ),  $D$  is the conductivity tensor,  $C_m$  is the specific membrane capacitance (50 pF),  $I_{ion}$  (given by the Nygren equations) is the total ionic current that crosses the membrane cells,  $V_m$  is the membrane potential, and  $I_{st}$  is the stimulus current density.

In this study the anisotropic ratio of conduction velocity was 2:1 for initial conditions, and a longitudinal conduction velocity of 60 cm/s was considered. The arrow in Figure 2 indicates the longitudinal direction of the virtual fiber orientation.

## 2.2 Simulation protocols

$S_1$ - $S_2$  protocol was implemented as follows: both control and remodeling models were excited by a train of ectopic beats with amplitude of 2.8 nA and duration of 6 ms, they were then applied in BB and IS areas ( $S_1$  dotted circles in the sidewall and superior wall of the model in Figure 2), simulating a continuous ectopic focus arriving from the superior vena cava of the right atrium through the interatrial bundles. It was applied to a cycle length of 300 ms; this value is within the data experimentally recorded of ectopic foci or used in atrial pacing.<sup>27,31</sup> After that, a burst

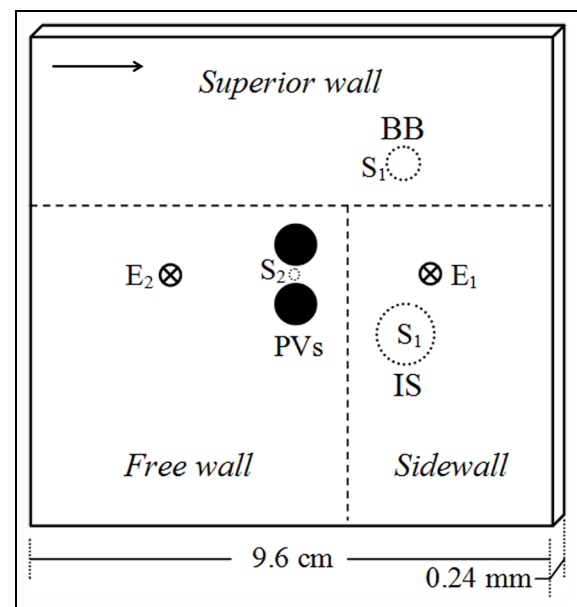


**Figure 2.** Two-dimensional model of human left atrial tissue including orifices for right pulmonary veins (PVs). BB is the zone where the Bachman bundle ends. IS is the zone where the interatrial septum ends. Pseudo-electrograms are registered in two locations “ $\otimes$ ” by two virtual electrodes (E1 and E2). Areas when the right atrium ectopic focus ( $S_1$ ) and PV ectopic focus ( $S_2$ ) are applied (dotted circles). The arrow indicates the longitudinal direction of the virtual fiber orientation.

of six ectopic beats ( $S_2$  dotted circles between the two right PVs in Figure 2) was applied during the repolarization phase of the 10th right atrium ectopic beat. PV ectopic beats were modeled by a supra-threshold stimulus with amplitude of 5.6 nA and duration of 6 ms to a localized area ( $5 \times 5$  nodes) between two orifices for the right PVs (dotted circles in the free wall of the model in Figure 2). They were applied to cycle length of 130 ms; this value is

taken from data recorded by Haissaguerre et al.<sup>12</sup> in PVs of patients with AF, range between 110 and 270 ms.

In order to investigate the influence of ectopic focus frequency, conduction velocity, and anisotropy on the reentrant patterns, the cycle length of the PV ectopic focus was increased to 260 and to 390 ms, for another study the velocity conduction was changed to 30 and to 90 cm/s, and for another one the anisotropic ratio was changed to 1:1 and to 3:1, respectively.

All simulations were finished 5 seconds after the first PV ectopic beat.

### 2.3 Simulated pseudo-unipolar electrograms

A unipolar electrogram (EGM) for a sheet of cells under the condition of uniform intracellular anisotropic resistivity was simulated as previously described.<sup>45</sup> The extracellular potential ( $\Phi_e$ ) is given by the following equation:

$$\Phi_e(r) = -\frac{1}{4\pi\sigma_e} \iiint \nabla' V_m(r') \cdot \nabla' \left[ \frac{1}{|r' - r|} \right] dv \quad (2)$$

where  $\nabla' V_m$  is the spatial gradient of transmembrane potential  $V_m$ ,  $\sigma_i$  is the intracellular conductivity,  $\sigma_e$  is the extracellular conductivity,  $|r' - r|$  is the distance between the source ( $x, y, z$ ) and the field point ( $x', y', z'$ ), and  $dv$  is the volume differential.

Pseudo-unipolar EGMs were computed every 1 ms for the period of 5 seconds after the first PV ectopic beat, for a simulated-electrode located in the sidewall (E1) and the free wall (E2) of the left atrium (“ $\otimes$ ” in Figure 2), 1 mm from the atrial surface.

### 2.4 Signal analysis

To analyze the frequency content of the model EGM, activity was sampled at 1 KHz for a 4-second window of 4096 points (the last 4 seconds of each simulation), providing a spectral resolution of 0.24 Hz. The signal was processed with a 40–250 Hz band-pass filter, rectified and low-pass filtered at 20 Hz. This filtering process extracts high-frequency components, and transforms a complex waveform into a series of atrial activations that underline the possible periodicity of the signal by reduction of the effects of varying EGM morphology or amplitude.<sup>46,47</sup> After that, spectral analysis of signals was performed with fast Fourier transform (FFT). The dominant frequency (DF) corresponded to the highest peak in the power spectrum. To measure the periodicity of the signal and the variability of frequency in the spectrum, the power of the DF and its harmonics was estimated by computing the area under the DF and its harmonics in the spectrum of the unfiltered signal. The ratio of this area to the total power was defined as the organization index (OI). A higher OI is

considered to represent less variability of frequency in a 4-second window.<sup>47,48</sup>

### 2.5 Numerical and computational methods

The mesh was built using Femap® from Siemens PLM software. Equations were numerically solved using EMOS® software. EMOS is a parallel code that implements the finite element method and operator splitting for solving the monodomain model. The time step was fixed to 0.02 ms. Simulation of 10 seconds took 12 hours on a computing node with a two 6-core Intel Xeon X5650 clocked at 2.66 GHz and 48 GB DDR3 RAM. EGM signal analysis was done using MATLAB® software.

## 3. Results

We evaluated the atrial tissue vulnerability to reentry using the 2D model under both physiological and remodeling conditions. We analyzed the reentrant patterns generated by the interaction between two ectopic foci, one of them a continuous focus that arrives from the right atrium through the BB and IS (S1) and the other one a burst of ectopic beats (S2) between the PVs. The right atrium ectopic focus was a continuous stimulus at cycle length of 300 ms and the PV ectopic focus was simulated by a train of six beats at a cycle length of 130 ms applied between the right PVs, as described in Section 2. When the right atrium ectopic focus excited the left atrium, it generated two activation wavefronts with elliptic form due to anisotropic tissue, as shown in the first snapshot in Figures 3(a) and (b) (right atrium activity).

In absence of electrical remodeling (physiological conditions) the first PV ectopic beat caused a unidirectional conduction block with a vulnerable window of 3 ms. The activation failed to propagate in the free wall direction, but it propagates in the sidewall direction. The wavefront traveled around the PVs and collided with its own refractory tail, becoming extinct due to the fact that the wavelength of excitation ( $\approx 8.6$  cm) was longer than the trajectory length (3.5 cm). Subsequently, some of the following PV ectopic beats were blocked by the right atrium ectopic activity, while the other ones generated wavefronts that also collided with their own refractory tail, becoming extinct (see Figure 3(a)). Therefore, it was not possible to obtain reentrant activity in physiological conditions.

In remodeled atrial tissue, the PV ectopic focus provoked complex reentrant wavefronts. After the first PV ectopic beat was applied, a unidirectional block was also generated; however, the width of the vulnerable window was higher (9 ms). In the first instant a reentry around the PVs was observed, because under the remodeling condition the wavelength ( $\approx 2.5$  cm) is shorter than the trajectory length (3.5 cm). After, the reentry around the PVs was fragmented in two daughter waves in the sidewall, each

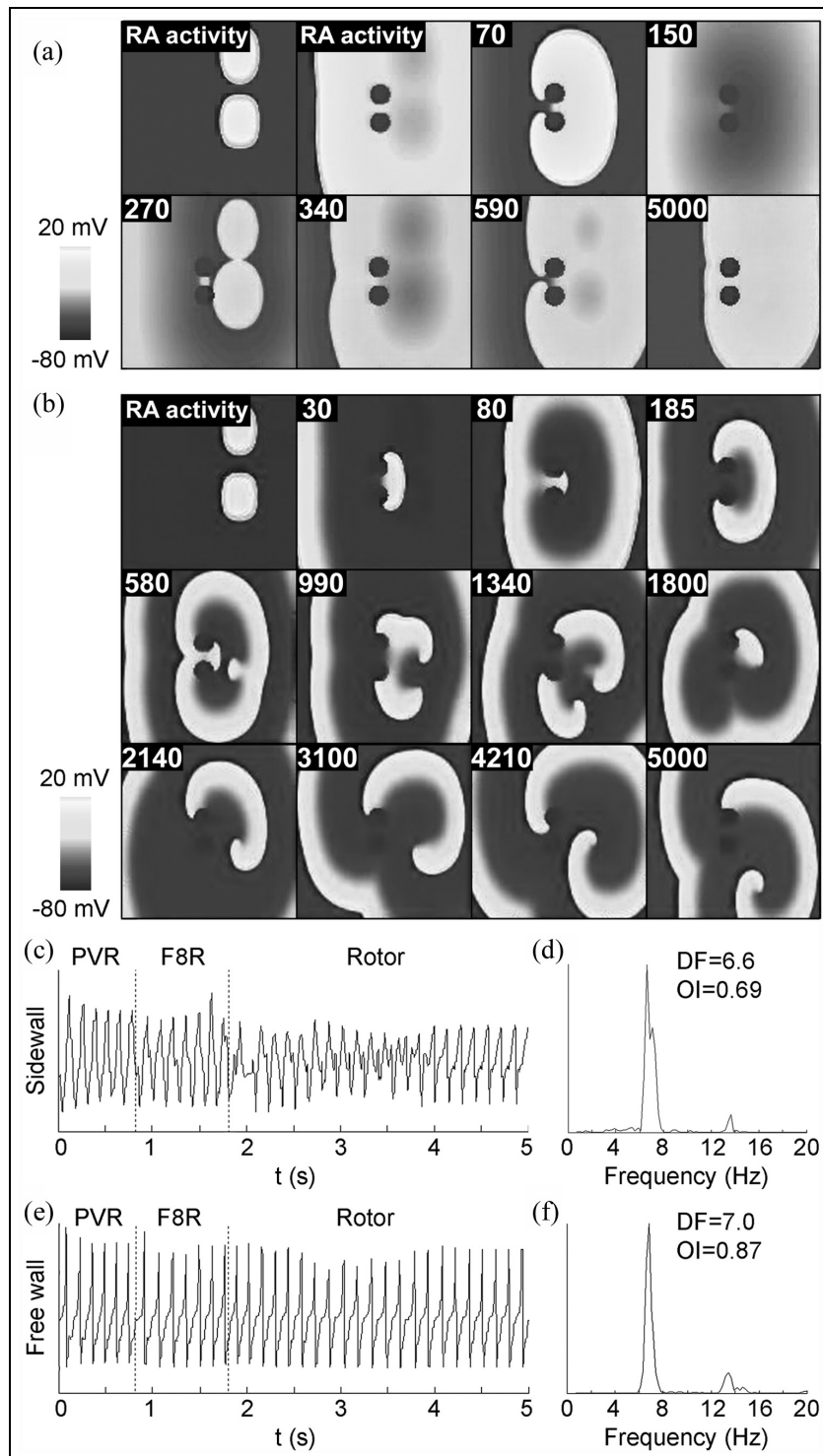


**Figure 3.** (a) Snapshots of membrane voltage in virtual physiological atrial tissue. The white color indicates depolarized voltage and the gray color represents repolarized voltage (times after the first pulmonary vein (PV) ectopic beat are indicated in milliseconds). The first, second, and eighth snapshots show right atrium ectopic activity activating the left atrium. The third to seventh snapshots represent the wavefront generated by PV ectopic beats. Some propagate around PVs and collide with their own refractory, while others are blocked by the right atrium ectopic activity or blocked due to the effective refractory period being longer. (b) Voltage snapshots in virtual remodeling tissue. A stable reentrant circuit around pulmonary veins (PVR) is generated by PV ectopic focus. As a result of the interaction of right atrium ectopic activity, episodes of figure-of-eight reentry (F8R) in the sidewall were initiated, and after that a rotor is generated. Pseudo-electrograms at (c) the free wall and (e) the sidewall and the corresponding power spectral densities ((d) and (f), respectively) registered during simulation in panel (b). The dominant frequency (DF) and organization index (OI) are shown.

one flanked by a singular point, inducing a figure-of-eight reentry, which was maintained for 1 second. After that, one of figure-of-eight reentry vortex was stabilized and converted in a rotor. The rotor was maintained during the remaining simulation, following a hypermeandering trajectory in the sidewall and turning in the clockwise direction (see Figure 3(b)).

Pseudo-EGMs were calculated at two points, one of them (E1) located in the sidewall and the other one located in the free wall (E2), as was mentioned in Section 2. They were calculated from the application of the first PV ectopic beat. It is possible to observe a higher EGM polymorphism (variability in size and shape) in the sidewall than in the free wall. The sidewall EGM displays single and double potentials, showing irregular activity characteristic of AF (see Figure 3(c)). On the contrary, the free wall EGM displays only single potentials (see Figure 3(e)). Figures 3(d) and (f) show the FFT analysis of the EGM in the sidewall and the free wall, respectively. The FFT analysis shows a DF gradient of 0.4 Hz between the free wall and the sidewall, with a single DF peak of 7.0 Hz in the free wall and a DF peak of 6.6 Hz in the sidewall. The OI was higher in the free wall (0.87) than in the sidewall (0.69), which represents more variability of frequency in the sidewall.

In summary, electrical remodeling and the anatomical structures of the atrium are important factors in reentry generation triggered by ectopic foci. In remodeled atria, the interaction between the continuous right atrium ectopic focus and a burst of PV ectopic beats initiated complex reentrant patterns, causing fibrillatory conduction. Higher EGM polymorphism is observed in the zone of tissue where complex reentrant patterns appeared. Our study suggests a DF gradient (0.4 Hz) even between nearby areas of regular and irregular activity in the left atrium.

### 3.1 Role of pulmonary vein ectopic focus frequency on the reentrant activity

PV ectopic foci with a wide range of frequencies have been experimentally observed.<sup>12,13,27,28,30,31</sup> To study the influence of the PV ectopic focus frequency on the reentrant activity, the cycle length of the PV ectopic burst was increased to 260 and 390 ms. The cycle length of the continuous ectopic activity arriving from the right atrium was maintained at 300 ms.

For a cycle length of 260 ms, the activity pattern observed was similar to that using a cycle length of 130 ms. After the application of PV ectopic beats, a reentrant wavefront propagating around the PVs degenerated in a figure-of-eight reentry and finally in a rotor. The rotor was also maintained following a hypermeandering trajectory in the sidewall. However, we can observe in Figure 4(a) that when the cycle length of the PV ectopic focus is increased

to 260 ms, the rotor starts later than when we used a cycle length of 130 ms.

The EGM showed that signal polymorphism was also greater in the sidewall (see Figure 4(a)) than in the free wall (not shown). FFT analysis (see Figure 4(e)) of the EGM shows a DF gradient of 0.6 Hz between the free wall and the sidewall, with a single DF peak of 7.1 Hz in the free wall and a DF peak of 6.5 Hz in the sidewall (see Figure 4(b)). The OI was also higher in the free wall (0.82) than in the sidewall (0.71).

On the other hand, when we increased the cycle length to 390 ms, the activation patterns were very different than using cycle lengths of 130 or 260 ms. After reentry around the PVs, figure-of-eight reentry was induced by the interaction with right atrium ectopic activity. However, this reentrant pattern was finished after four complete reentries. In the last 3 seconds of the simulations, the sidewall and the free wall EGM showed periodic single potentials separated by a baseline (see Figure 4(c)), which correspond to regular activation of a lower frequency than the reentrant activity. The FFT analyses of the EGM in the free wall and the sidewall (see Figure 4(d)) show DF peaks of 3.4 Hz in both zones (see Figure 4(e)); the OI was similar in the free wall (0.9) and in the sidewall (0.88), which corresponds to the stable right atrium ectopic activity.

For right atrium continuous ectopic activity with a basic cycle length of 300 ms, our results show that the interaction of this ectopic activity and a burst of ectopic beats in the PV generated reentrant activity when the frequency of the PV ectopic burst was higher than the right atrium ectopic activity. On the other hand, it is possible to observe that the morphology and periodicity of the EGM complexes during reentrant activity are dissimilar to periodic focal activity. The DF and OI present gradients (between the sidewall and the free wall) when the atrial tissue is being excited by an irregular reentrant activity, whereas periodic activity due to the continuous ectopic focus does not presents any gradients, and the OI values are higher (see Figure 4(f)).

### 3.2 Role of conduction velocity on the reentrant activity

Some studies have suggested that a slow conduction velocity around the PVs<sup>27,39,41,49</sup> contributes to favor the appearance of multiple reentrant wavelets in this region. In order to investigate the influence of the conduction velocity on the reentrant activity, the conduction velocity was decreased to 30 cm/s, and increased to 90 cm/s, maintaining a 2:1 anisotropic ratio. The burst of 6 PV ectopic beats was applied at a cycle length of 130 ms and the cycle length of right atrium ectopic activity was maintained at 300 ms.

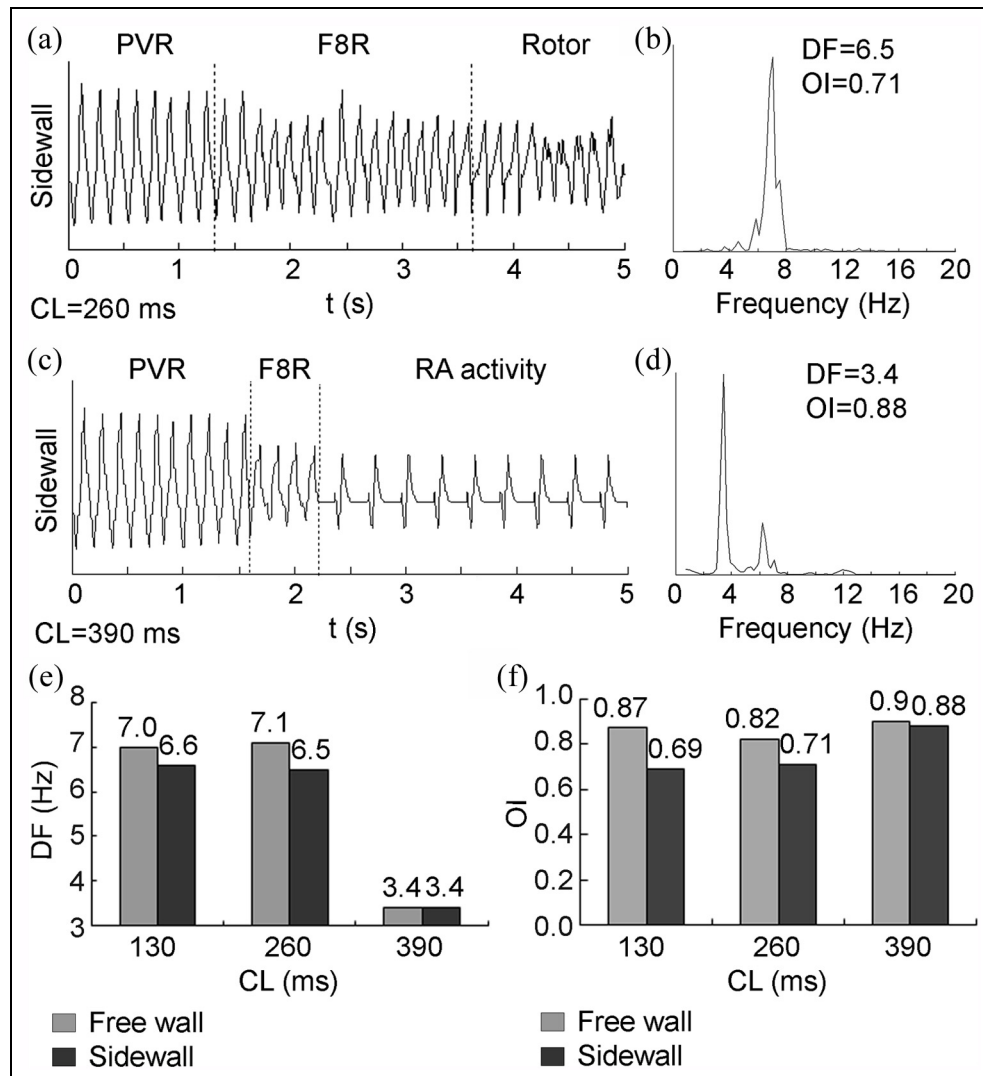


**Figure 4.** Pseudo-electrogram at the sidewall of the virtual tissue at (a) focal cycle length of 260 ms and (c) 390 ms. Episodes of stable reentry around pulmonary veins (PVR), figure-of-eight reentry (F8R), rotor, and right atrium ectopic activity are shown. (b) and (d) The corresponding power spectral densities. The dominant frequency (DF) and organization index (OI) are shown. Bar plots of (e) DF and (f) OI in the free wall (gray) and the sidewall (black) at different cycle lengths.

Decreasing the conduction velocity to 30 cm/s, the activity pattern observed (see Figure 5(a) for the sidewall pattern) was similar to that using a conduction velocity of 60 cm/s (see Figure 3(c)). After the application of the ectopic burst in the PV, the reentrant wavefront propagated around the PVs, followed by a figure-of-eight reentry degenerated in a rotor in the sidewall.

Again, the EGM showed signal polymorphism greater in the sidewall than in the free wall. Figure 5(b) shows the FFT analysis of the EGM in the sidewall. It shows a single DF peak of 5.8 Hz, while the DF peak in the free wall is 6.3 Hz (not shown). These results indicate a DF gradient of 0.5 Hz between the free wall and the sidewall (see Figure 5(e)). DF values are slightly lower than those obtained

using a conduction velocity of 60 cm/s; this is mainly due to the conduction velocity decrease in the virtual atrial tissue. The OI was also higher in the free wall (0.79) than in the sidewall (0.63) (see Figure 5(f)).

On the other hand, when we increased the conduction velocity to 90 cm/s, the activation patterns were different than using a conduction velocity of 60 or 30 cm/s. The reentry around PVs generated by the PV ectopic focus was the driver that maintained the tachycardia. In this case, rotor activity was not generated. The reentry around the PVs took the control of the atrial activation and it was maintained during the entire simulation. Only a figure-of-eight reentry was induced by the interaction of the right atrium ectopic activity wavefront with the reentrant

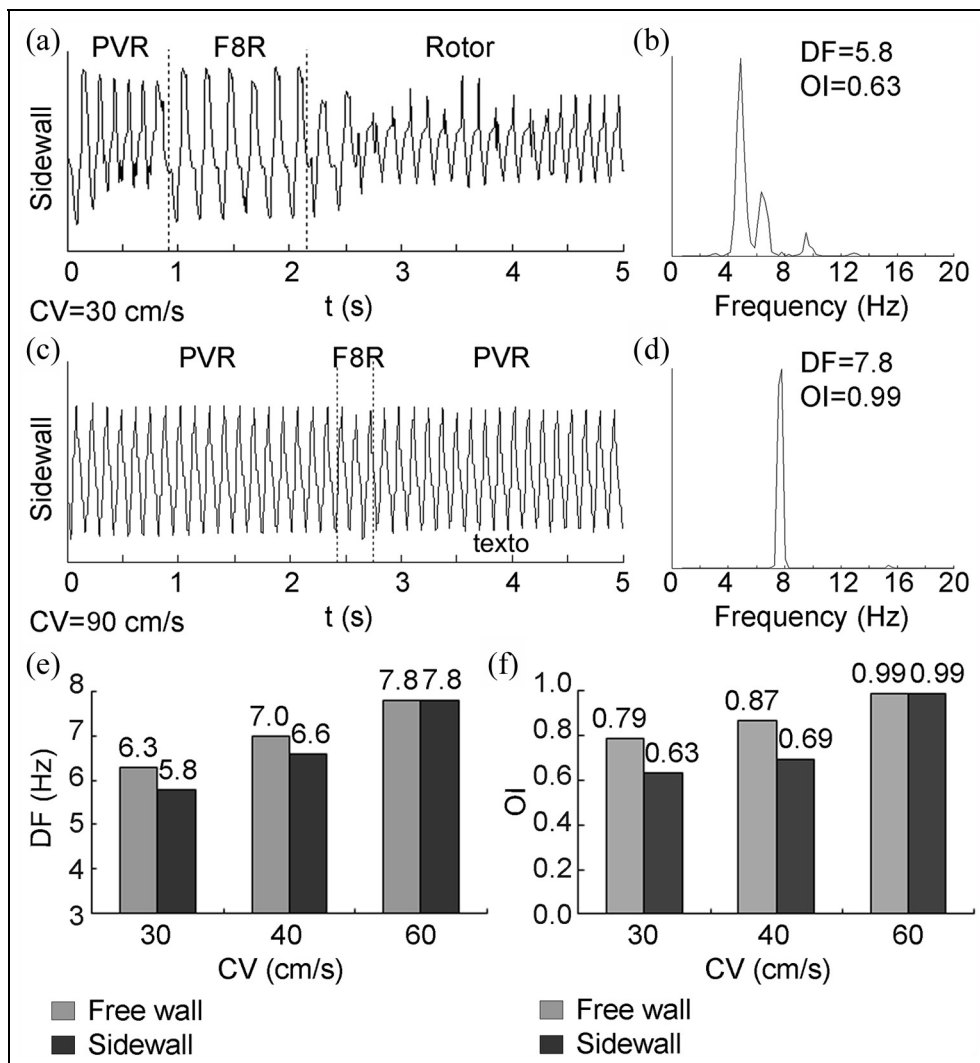


**Figure 5.** Pseudo-electrogram at the sidewall of the virtual tissue at (a) conduction velocities (CVs) of 30 cm/s and (c) 90 cm/s. Episodes of stable reentry around pulmonary veins (PVR), figure-of-eight reentry (F8R), rotor, and right atrium ectopic activity are shown. (b) and (d) The corresponding power spectral densities. The dominant frequency (DF) and organization index (OI) are shown. Bar plots of (e) DF and (f) OI in the free wall (gray) and the sidewall (black) at different cycle lengths.

activation at 2.5 seconds, approximately. However, this reentrant pattern was finished after two complete reentries.

The pseudo-EGM in both the sidewall (see Figure 5(c)) and the free wall (not shown) displays single potentials, showing stable and regular atrial activation that appear in the FFT analyses as single DF peaks of 7.8 Hz and a high OI value in both zones (0.99) (see Figure 5(d)).

In summary, in remodeling tissue with normal and low conduction velocities (60 cm/s and 30 cm/s) patterns of fibrillatory conduction are shown generating a DF and OI gradients. However, when the conduction velocity is increased (to 90 cm/s) only a focal atrial tachycardia pattern is observed and gradients are not generated (see Figures 5(e) and (f)).

### 3.3 Role of anisotropic ratio on the reentrant activity

Experimental studies suggest that the intrinsic anisotropy of the tissue contributes to generating wavebreaks and fibrillatory activity.<sup>40-42</sup> In order to investigate the influence of anisotropy on the reentrant activity, the ratio of conductivities was modified.

We used a 3:1 anisotropic model, with longitudinal and transversal conduction velocities of 90 and 30 cm/s, respectively, and an isotropic (1:1) model, with a conduction velocity of 60 cm/s in both directions. A burst of six PV ectopic beats at a cycle length of 130 ms was applied, while the cycle length of the right atrium ectopic focus was maintained at 300 ms.



Increasing the anisotropic ratio to 3:1, the burst of PV ectopic beats generated a reentrant wavefront around the PVs and figure-of-eight reentry. This reentrant pattern was maintained for very short time. After that, another functional figure-of-eight reentry was generated, initiating two figure-of-eight reentry patterns in the sidewall. This reentry with four singular points is called quatrefoil reentry (see Figure 6(a)). This reentrant pattern was maintained during the remaining simulation.

The sidewall EGM displays a few single potentials; most are double and fragmented potentials (see Figure 6(b)). The unstable and very irregular activity in the sidewall appears in the FFT analysis as multiple frequency peaks from 3.6 to 9.8 Hz (see Figure 6(c)), corresponding to a very chaotic fibrillatory conduction. Figure 6(f) shows a DF gradient of 0.4 Hz between the free wall (6.8 Hz) and the sidewall (6.4 Hz). OIs were very low (0.67 in the free wall and 0.41 in the sidewall) being lower in the sidewall (see Figure 6(g)), which represents greater variability of frequency.

In the isotropic tissue, the reentry around the PVs generated by the PV ectopic burst was the driver that maintained the tachycardia; only two episodes of figure-of-eight reentries of very short duration (from one to three complete reentries) were observed. In this case rotors were not generated.

The pseudo-EGM in both the sidewall (see Figure 6(d)) and the free wall (not shown) display single potentials, showing stable and regular atrial activation, which appear in the FFT analyses (see Figure 6(e)) as single DF peaks of 7.3 Hz in both zones and high OI values (0.99 in the free wall and 0.98 in the sidewall) (see Figures 6(f) and (g)).

In our simulations, complex reentrant patterns appeared using 2:1 and 3:1 anisotropic remodeling atrial tissue, but not in isotropic atrial tissue. In addition, as the anisotropy of the tissue became higher, more reentrant circuits were obtained and the reentrant activity pattern was more chaotic.

## 4. Discussion

In the present study, we investigated the influence of focus frequency, conduction velocity, and anisotropy on fibrillatory pattern generation during the interaction of two ectopic foci under electrical remodeling conditions. For this purpose, a 2D computer model of electrical activity of human left atrial tissue, including two orifices for right PVs, was developed.

### 4.1 Effect of the interaction of two ectopic foci

Our simulations showed that electrical remodeling shortened atrial APD, as has been widely reported. It reduced ERP, which facilitated reentry generation, showing the

pro-arrhythmic effect of remodeling. Different experimental studies have demonstrated that remodeling is a substrate necessary to maintain reentrant patterns.<sup>15,34–36</sup> In addition, there are a great number of experimental results that have shown reentrant patterns associated with ectopic activity observed within or near to PVs.<sup>13,39</sup> Several investigators have demonstrated the presence of focal activity in the PVs, which is responsible for atrial tachycardia.<sup>12–14,19,27,28,38</sup> Nevertheless, many doubts still exist about the role of the ectopic foci: is it limited to initiate reentries? Clinical studies developed by Haissaguerre et al.<sup>12</sup> demonstrated that a short burst of two or more repetitive focal discharges can generate spontaneous AF, but they were not required to maintain it. However, studies by Chen et al.<sup>13</sup> and Kumagai et al.<sup>28</sup> showed the role of ectopic foci in the initiation and maintenance of reentries associated with AF.

Our results support the broadly accepted theory that focal activity acting near PVs is an initiator of reentrant mechanisms in vulnerable tissue (remodeling tissue). This fact would actually explain that in clinical practice, the elimination of the focus origin does not obtain such satisfactory results in the elimination of arrhythmia as those obtained from procedures destined to isolate the PVs in the surrounding atrial myocardium, which is more compatible with an elimination of the necessary substrate for a reentrant mechanism than with the elimination of initiator/maintainer beats.

In our study, when we applied a burst of ectopic beats, a reentry around the PVs was generated only in a remodeling atrial tissue. The PVs acted as an obstacle and the ERP decreased by the effect of the electrical remodeling, facilitating the maintenance of reentrant activity. These results are in agreement with several studies that have reported the importance of anatomical obstacles (for example, PVs) for reentrant wave generation.<sup>13,14,50,51</sup>

Although AF is initiated from focal triggers most commonly localized to the atrialization of PVs,<sup>12,13,27,28</sup> ectopic foci have been recorded in other regions. Besides, it has been demonstrated that it is possible that multiple ectopic foci co-exist. A study<sup>31</sup> was made of 293 patients with ectopic beats initiating AF, of whom 20% had both PV and non-PV ectopic beats initiating AF. In a study with 27 patients,<sup>30</sup> all of them had multiple AF foci, of whom 17 patients had AF from PV and superior vena cava foci. In our simulations, with conduction velocities of 60 or 30 cm/s and 2:1 anisotropy, the interaction of the reentry around the PV with continuous right atrium ectopic activity caused wavebreaks, and a figure-of-eight reentry was induced. This reentry pattern has been observed experimentally<sup>52,53</sup> and in computational models of heart tissue.<sup>54</sup> An *in vitro* and *in silico* study<sup>55</sup> showed that waves emitted by faster pacemakers break up over the slower pacemakers to form reentrant waves, concluding that pacemaker interactions can lead to the complex wave dynamics

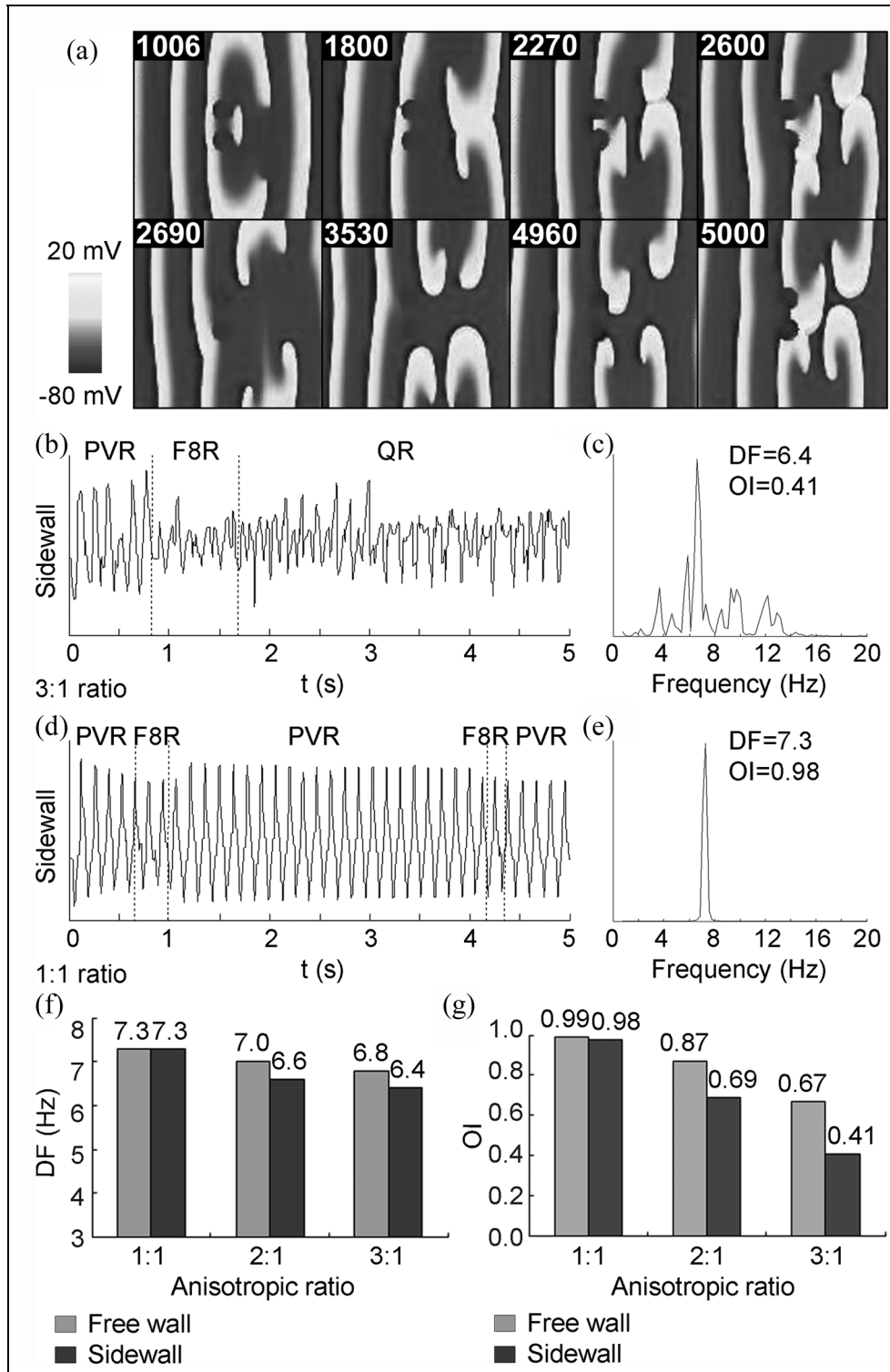


**Figure 6.** (a) Snapshots of membrane voltage in virtual remodeling atrial tissue with a 3:1 anisotropic ratio, showing quatrefoil reentry. The white color indicates depolarized voltage and the gray color indicates repolarized voltage (times after the first pulmonary vein (PV) ectopic beat are indicated in milliseconds). (b) Pseudo-electrogram at the sidewall of the virtual tissue at anisotropic ratios of 3:1 and (d) 1:1. Episodes of stable reentry around pulmonary veins (PVR), figure-of-eight reentry (F8R), and quatrefoil reentry (QR) are shown. (c) and (e) The corresponding power spectral densities. The dominant frequency (DF) and organization index (OI) are shown. Bar plots of (f) DF and (g) OI in the free wall (gray) and the sidewall (black) at different cycle lengths.

seen in certain types of cardiac arrhythmias. A study of a 2D model of atrial tissue<sup>56</sup> showed that when the interaction between ectopic focal activity and reentry occurs, reentry breaks up, forming multiple wavelets. A study of a 3D model of human atria<sup>57</sup> simulated spontaneous firings of ectopic foci coupled with sinus activity, where the sites and likelihood of reentry induction varied according to the ectopic focus location and timing. The size of the vulnerable window was largest for PV foci.

In our study, the figure-of-eight reentry degenerated in a rotor activity in the sidewall that stays during the remaining simulation. These results are in agreement with the “rotor hypothesis” proposed by Jalife.<sup>24</sup> This hypothesis suggests that the AF is triggered by a burst of ectopic beats originated in the PVs; their wavefronts would fragment, generating two vortices rotating in opposite senses (figure-of-eight reentry). Finally, one of these vortices would become stabilized in the atrial wall generating a functional reentry or a rotor, which would act as mechanism of maintenance activating the local tissue to high frequency and of highly regular form, generating wavefronts that would fragment and propagate in highly recurrent directions.

Experimental studies have demonstrated that the EGM morphology and FFT technique can quickly identify activation patterns that may provide evidence of an underlying arrhythmia mechanism or mechanisms. The continuous change in direction and width of fibrillation waves explains the characteristic spatiotemporal variations in morphology of the fibrillation EGM. In our simulations, signal polymorphism of the EGM calculated was greater in proximity to irregular activity (figure-of-eight reentry and rotor), displaying double potentials. Experimental studies have shown that the polymorphism of the signals recorded is greater in areas of irregular and unstable activity during fibrillatory conduction. Multiple potentials have been observed during AF episodes in areas where collisions and blockages occur.<sup>19–22,58,59</sup>

We obtained a DF gradient from the sidewall to the free wall; this indicates that the activation pattern is heterogeneous throughout the region being characterized, consistent with the presence of AF. FFT analyses of the sidewall showed two or three frequency peaks as a consequence of unstable and irregular activity in this region. These results agree with experimental studies.<sup>19–21,53,60</sup> A study with dogs<sup>59</sup> showed that during an AF episode due to a stable reentrant circuit around the PVs they obtained similar DF values ( $\approx 7.3$  Hz) in the region near to the PVs and different DF values (from 6.7 to 6.2 Hz) in remote areas, due to the multiple reentrant waves, showing a gradient of PV to left atrial activation of  $\approx 0.6$  Hz. They found multiple or broadband frequency peak in areas with unstable and irregular activation.

## 4.2 Role of pulmonary vein ectopic focus frequency on the reentrant activity

Experimentally ectopic activity at a wide range of cycle length has been observed (from 110 to 1000 ms). Cycle lengths of 108–280 ms of focal discharges of about 340 beats per minute (bpm) have been measured.<sup>12,13,27–31</sup> In some cases these foci are very rapid. In our simulations, the ectopic focus applied to cycle lengths of 130 and 260 ms began reentrant mechanisms, showing fibrillatory activity. This result is in agreement with Haissaguerre et al.,<sup>61</sup> which registered ectopic foci with a range of cycle lengths from 110 to 270 ms that generated AF in patients.

When the ectopic focus cycle length was increased (390 ms) above the right atrium ectopic focus cycle length (300 ms), all reentrant activity was finished at a few seconds of simulation, staying only the right atrium ectopic activity in the tissue, taking control of the atrial activation. In a study using a three-dimensional (3D) model of human atria,<sup>57</sup> atrial flutter or AF could be initiated by rapid firing of ectopic foci with only a few beats (10), within the range  $160 \leq \text{cycle length} \leq 200$  ms.

In a study with dogs,<sup>27</sup> discrete foci were discovered in two different locations, with one focus being significantly faster than the other (330 versus 1000 ms cycle length). The faster focus was transient and was inducible only with burst atrial pacing. In contrast, the slower focus fired continuously but seemed to be transiently suppressed in the presence of the faster focus. In our case, when the continuous right atrium ectopic activity is the faster focus, this focus takes control of the atrial activation. The change from reentrant activity to right atrium ectopic activity was observed clearly in the EGM obtained. Right atrium ectopic activity was characterized for single potentials to a slower constant frequency of 3.4 Hz.

## 4.3 Role of conduction velocity on the reentrant activity

Some studies have shown that the conduction velocity around PVs is slow,<sup>27,38,39,41,49</sup> which could contribute to the generation of chaotic activity. In a study carried out by Arora et al.<sup>27</sup> in dogs observed a conduction velocity slower in the proximal region of PVs compared with the remaining atrial tissue (45.8 cm/s versus 67.6 cm/s in the endocardium and 31.3 cm/s versus 90.2 cm/s in the epicardium).

On the basis of these studies, a normal conduction velocity of 60 cm/s for our simulations was selected. The burst of ectopic focus applied generated fibrillatory conduction. When this conduction velocity was decreased, fibrillatory activity also was generated. However, when the conduction velocity was increased to similar values to those of

the atrial muscle bundles, no fibrillatory conduction was observed. These results suggest that in remodeling tissue, with normal and low conduction velocities it is possible to obtain fibrillatory patterns of figure-of-eight reentries and rotors in proximity to PVs, which is in agreement with studies that have reported that a slow conduction velocity decreases the wavelength and therefore favors AF stability.<sup>15</sup> On the contrary, when the conduction velocity increases, it is more likely to observe a focal atrial tachycardia pattern. In our simulations with a conduction velocity of 90 cm/s, stable reentry around PVs was generated. The EGM showed single potentials and the FFT analyses showed a single DF peak at the same value in the free wall and the sidewall. This indicates that the activation pattern is homogeneous throughout the region being characterized, following a driver in a 1:1 manner, consistent with the presence of focal atrial tachycardia.<sup>17</sup> These results agree with experimental studies.<sup>30,53,60</sup> A study with dogs<sup>59</sup> showed the same DF value in all recording sites during focal atrial tachycardia (5.62 Hz).

#### 4.4 Role of anisotropic tissue in the reentrant activity

In our study the anisotropy of the tissue helps to maintain the fibrillatory activity. This is in agreement with experimental studies<sup>40-42</sup> that have demonstrated that the intrinsic anisotropy of the tissue helps the generation of wavebreak and fibrillatory conduction. Our results showed that fibrillatory conduction was obtained only in 2:1 and 3:1 anisotropic atrial tissue. On the contrary, in isotropic atrial tissue fibrillatory conduction was not generated, but a focal atrial tachycardia pattern was observed.

When we increased the anisotropy, this increased the number of wavebreaks and thus the complexity of the activation pattern. The figure-of-eight reentry was converted to a reentry mechanism of four lobes; Lin et al.<sup>62</sup> was the first to observe this experimentally in a rabbit heart. The quatrefoil reentry caused more irregular EGM forms with double and fragmental potentials resulting from dissociation and picoting of fibrillation waves. These types of potentials are seen more frequently<sup>58</sup> in patients with chronic AF, recorded from parts of the left atrium and the PVs. FFT analysis showed multiple frequency peaks (> three peaks) as a consequence of chaotic activity. A study with dogs<sup>59</sup> found broadband with multiple frequency peaks corresponding to fibrillatory conduction caused by multiple unstable reentrant circuits.

#### 4.5 Clinical implications

Our simulations showed that the incidence of arrhythmias depends on multiple factors: electrical remodeling, interaction between ectopic foci, ectopic foci frequency, conduction velocity, and anisotropy of the atrial tissue. This

observation gives a theoretical frame and support to experimental and clinical observations of AF and focal atrial tachycardia generation. The model reflects the clinical picture found in some cases of AF, exhibiting fast and irregular activity at locations where wave generation and wavebreaks are observed, which cause a DF gradient in nearby areas within the left atrium.

Hence, the region surrounding the PVs and the sidewall in our model constitute a substrate for AF and can maintain the arrhythmia after its initiation. Therefore, from a therapeutic point of view, elimination of the reentrant circuits, that is, more peristial ablation of the PVs, including the region surrounding the ostium and part of the sidewall, should be more efficient than isolation of only the veins, which would eliminate only the trigger.

#### 4.6 Limitations of the study

Finally, some limitations should be mentioned. Our 2D simulations do not consider possible alterations in gap junctions or APD heterogeneity, all which may play important roles in the maintenance of AF. Other modeling studies could incorporate these complexities (gap junctions and heterogeneity), perhaps individually or in combination, and then study the resultant effects on AF maintenance and/or termination. There is a slight delay between activity from BB and IS that was not considered; future studies could incorporate this delay. We included two PVs in the model in order to study the effect of the interaction between an ectopic activity from the right atrium and a single ectopic focus generated between two PVs; however, it would be interesting to perform a similar study in a more realistic 2D model including four PVs.

In addition, our present work needs to be extended to more realistic 3D, anatomically detailed models of the human atria. FFT analysis is not able to distinguish the difference between a rotor and a figure-of-eight reentry. Since both mechanisms have an irregular activation pattern, the FFT analysis will show broadbands with multiple frequency peaks in both mechanisms. Also, reliable use of FFT analysis of an auricular EGM requires adequate recording resolution to discriminate activation patterns.

Despite the above limitations, our results give useful insights into the electrophysiological parameters that determine the initiation and maintenance of fibrillatory conduction in a simulated 2D sheet of human atrial cells, under chronic AF conditions.

## 5. Conclusions

Our results support the broadly accepted theory that ectopic activity near to the PVs, acting in remodeling tissue, is an initiator of reentrant mechanisms. These reentrant circuits can generate fibrillatory activity when interacting with an ectopic focus arising from the right atrium and

under the following conditions: high PV ectopic focus frequency, slow conduction velocity, and anisotropic tissue. Analyses of EGM polymorphism permit one to know in which zone of tissue unstable activity exists. Our study suggests a DF gradient between nearby areas of regular and irregular activity in the left atrium.


### Declaration of conflicting interest

The authors declare that there is no conflict of interest.

### Funding

This work was partially supported by the Dirección General de Política Científica de la Generalitat Valenciana (PROMETEU 2016/088) and the University of Medellín.

### ORCID iD

Catalina Tobón  <https://orcid.org/0000-0002-0578-329X>

### References

1. Fuster V, Rydén LE, Cannom DS, et al. ACC/AHA/ESC 2006 guidelines for the management of patients with atrial fibrillation. *Circulation* 2006; 114: 700–752.
2. Stewart S, Hart CL, Hole DJ, et al. A population-based study of the long-term risks associated with atrial fibrillation: 20-year follow-up of the Renfrew/Paisley study. *Am J Med* 2002; 113: 359–364.
3. Wolf PA, Abbott RD and Kannel WB. Atrial fibrillation as an independent risk factor for stroke: the Framingham Study. *Stroke* 1991; 22: 983–988.
4. Krahn AD, Manfreda J, Tate RB, et al. The natural history of atrial fibrillation: incidence, risk factors, and prognosis in the manitoba follow-up study. *Am J Med* 1995; 98: 476–484.
5. Zoni-Berisso M, Lercari F, Carazza T, et al. Epidemiology of atrial fibrillation: European perspective. *Clin Epidemiol* 2014; 6: 213–220.
6. Corradi D. Atrial fibrillation from the pathologist's perspective. *Cardiovasc Pathol* 2014; 23(2): 71–84.
7. Kishore A, Vail A, Majid A, et al. Detection of atrial fibrillation after ischemic stroke or transient ischemic attack: a systematic review and meta-analysis. *Stroke* 2014; 45: 520–526.
8. Knecht S, Oelschläger C, Duning T, et al. Atrial fibrillation in stroke-free patients is associated with memory impairment and hippocampal atrophy. *Eur Heart J* 2008; 29: 2125–2132.
9. Thrall G, Lane D, Carroll D, et al. Quality of life in patients with atrial fibrillation: a systematic review. *Am J Med* 2006; 119: 448.e1–19.
10. Steinberg BA, Kim S, Fonarow GC, et al. Drivers of hospitalization for patients with atrial fibrillation: results from the Outcomes Registry for Better Informed Treatment of Atrial Fibrillation (ORBIT-AF). *Am Heart J* 2014; 167: 735–742.e2.
11. Kirchhof P, Benussi S, Kotecha D, et al. 2016 ESC Guidelines for the management of atrial fibrillation developed in collaboration with EACTS. *Europace* 2016; 18(11): 1609–1678.
12. Haissaguerre M, Jais P, Shah DC, et al. Spontaneous initiation of atrial fibrillation by ectopic beats originating in the pulmonary veins. *N Engl J Med* 1998; 339: 659–666.
13. Chen SA, Hsieh MH, Tai CT, et al. Initiation of atrial fibrillation by ectopic beats originating from the pulmonary veins: electrophysiological characteristics, pharmacological responses, and effects of radiofrequency ablation. *Circulation* 1999; 100: 1879–1886.
14. Chen YJ, Chen SA, Chang MS, et al. Arrhythmogenic activity of cardiac muscle in pulmonary veins of the dog: Implication for the genesis of atrial fibrillation. *Cardiovasc Res* 2000; 48: 265–273.
15. Nattel S, Burstein B and Dobrev D. Atrial remodeling and atrial fibrillation: mechanisms and implications. *Circulat Arrhyth Electrophysiol* 2008; 1: 62–73.
16. de Vos CB, Pisters R, Nieuwlaar R, et al. Progression from paroxysmal to persistent atrial fibrillation. Clinical correlates and prognosis. *J Am Coll Cardiol* 2010; 55: 725–731.
17. De Groot NMS and Schalij MJ. Fragmented, long-duration, low-amplitude electrograms characterize the origin of focal atrial tachycardia. *J Cardiovasc Electrophysiol* 2006; 17: 1086–1092.
18. Pison L, Tilz R, Jalife J, et al. Pulmonary vein triggers, focal sources, rotors and atrial cardiomyopathy: Implications for the choice of the most effective ablation therapy. *J Intern Med* 2016; 279: 449–456.
19. Sanders P, Berenfeld O, Hocini M, et al. Spectral analysis identifies sites of high-frequency activity maintaining atrial fibrillation in humans. *Circulation* 2005; 112: 789–797.
20. Hansen BJ, Zhao J, Csepe TA, et al. Atrial fibrillation driven by micro-anatomic intramural re-entry revealed by simultaneous sub-epicardial and sub-endocardial optical mapping in explanted human hearts. *Eur Heart J* 2015; 36: 2390–2401.
21. Narayan SM, Krummen DE, Shivkumar K, et al. Treatment of atrial fibrillation by the ablation of localized sources. *J Am Coll Cardiol* 2012; 60: 628–636.
22. Mandapati R, Skanes A, Chen J, et al. Stable microreentrant sources as a mechanism of atrial fibrillation in the isolated sheep heart. *Circulation* 2000; 101: 194–199.
23. Mansour M, Mandapati R, Berenfeld O, et al. Left-to-right gradient of atrial frequencies during acute atrial fibrillation in the isolated sheep heart. *Circulation* 2001; 103: 2631–2636.
24. Jalife J. Rotors and spiral waves in atrial fibrillation. *J Cardiovasc Electrophysiol* 2003; 14: 776–780.
25. Reumann M, Bohnert J, Osswald B, et al. Multiple wavelets, rotors, and snakes in atrial fibrillation—a computer simulation study. *J Electrocardiol* 2007; 40: 328–334.
26. Ugarte J, Orozco-Duque A, Tobón C, et al. Dynamic approximate entropy electroanatomic maps detect rotors in a simulated atrial fibrillation model. *PLoS One* 2014; 9: e114577.
27. Arora R, Verheule S, Scott L, et al. Arrhythmogenic substrate of the pulmonary veins assessed by high-resolution optical mapping. *Circulation* 2003; 107: 1816–1821.
28. Kumagai K, Gondo N, Matsumoto N, et al. New technique for simultaneous catheter mapping of pulmonary veins for

- catheter ablation in focal atrial fibrillation. *Cardiology* 2000; 94: 233–238.
29. Nanthakumar K, Lau YR, Plumb VJ, et al. Electrophysiological findings in adolescents with atrial fibrillation who have structurally normal hearts. *Circulation* 2004; 110: 117–123.
  30. Lin WS, Tai CT, Hsieh MH, et al. Catheter ablation of paroxysmal atrial fibrillation initiated by non-pulmonary vein ectopy. *Circulation* 2003; 107: 3176–3183.
  31. Lee SH, Chen SA and Tai CT. Predictors of non-pulmonary vein ectopic beats initiating paroxysmal atrial fibrillation - implication for catheter ablation. *Acta Cardiologica Sinica* 2007; 46(6): 13–19.
  32. Bosch RF, Zeng X, Grammer JB, et al. Ionic mechanisms of electrical remodeling in human atrial fibrillation. *Cardiovasc Res* 1999; 44: 121–131.
  33. Workman AJ, Kane KA and Rankin AC. The contribution of ionic currents to changes in refractoriness of human atrial myocytes associated with chronic atrial fibrillation. *Cardiovasc Res* 2001; 52: 226–235.
  34. Wijffels MC, Kirchhof CJ, Dorland R, et al. Atrial fibrillation begets atrial fibrillation. A study in awake chronically instrumented goats. *Circulation* 1995; 92: 1954–1968.
  35. Schotten U, Verheule S, Kirchhof P, et al. Pathophysiological mechanisms of atrial fibrillation: a translational appraisal. *Physiol Rev* 2011; 91: 265–325.
  36. Veenhuizen GD, Simpson CS and Abdollah H. Atrial fibrillation. *Can Med Assoc J* 2004; 171: 755–760.
  37. Weiss JN, Qu Z and Shivkumar K. Ablating atrial fibrillation: a translational science perspective for clinicians. *Heart Rhythm* 2016; 13: 1868–1877.
  38. Jais P, Haissaguerre M, Shah DC, et al. A focal source of atrial fibrillation treated by discrete radiofrequency ablation. *Circulation* 1997; 95: 572–576.
  39. Belhassen B, Glick A and Viskin S. Reentry in a pulmonary vein as a possible mechanism of focal atrial fibrillation. *J Cardiovasc Electrophysiol* 2004; 15: 824–828.
  40. Wilders R, Wagner MB, Golod DA, et al. Effects of anisotropy on the development of cardiac arrhythmias associated with focal activity. *Pflugers Arch Eur J Physiol* 2000; 441: 301–312.
  41. Zhao J, Butters TD, Zhang H, et al. An image-based model of atrial muscular architecture effects of structural anisotropy on electrical activation. *Circulat Arrhythmia Electrophysiol* 2012; 5: 361–370.
  42. Aslanidi OV, Boyett MR, Dobrzynski H, et al. Mechanisms of transition from normal to reentrant electrical activity in a model of rabbit atrial tissue: interaction of tissue heterogeneity and anisotropy. *Biophys J* 2009; 96: 798–817.
  43. Nygren A, Fiset C, Firek L, et al. Mathematical model of an adult human atrial cell: the role of K<sup>+</sup> currents in repolarization. *Circ Res* 1998; 82: 63–81.
  44. Ho SY, Sanchez-Quintana D, Cabrera JA, et al. Anatomy of the left atrium: implications for radiofrequency ablation of atrial fibrillation. *J Cardiovasc Electrophysiol* 1999; 10: 1525–1533.
  45. Tobón C, Orozco-Duque A, Ugarte J, et al. Complexity of atrial fibrillation electrograms through nonlinear signal analysis: in silico approach. In: Michael KA (ed.) *Interpreting cardiac electrograms - from skin to endocardium*. London: InTech, 2017, pp.137–168.
  46. Takahashi Y, Sanders P, Jais P, et al. Organization of frequency spectra of atrial fibrillation: relevance to radiofrequency catheter ablation. *J Cardiovasc Electrophysiol* 2006; 17: 382–388.
  47. Tobón C, Rodríguez JF, Ferrero JM Jr et al. Dominant frequency and organization index maps in a realistic three-dimensional computational model of atrial fibrillation. *Europace* 2012; 14: v25-v32.
  48. Everett TH, Wilson EE, Verheule S, et al. Structural atrial remodeling alters the substrate and spatiotemporal organization of atrial fibrillation: a comparison in canine models of structural and electrical atrial remodeling. *Am J Physiol Heart Circ Physiol* 2006; 291: H2911–23.
  49. Jais P, Hocini M, Macle L, et al. Distinctive electrophysiological properties of pulmonary veins in patients with atrial fibrillation. *Circulation* 2002; 106: 2479–2485.
  50. Ikeda T, Yashima M, Uchida T, et al. Attachment of meandering reentrant wave fronts to anatomic obstacles in the atrium. Role of the obstacle size. *Circ Res* 1997; 81: 753–764.
  51. Wieser L, Nowak CN, Tilg B, et al. Mother rotor anchoring in branching tissue with heterogeneous membrane properties. *Biomed Tech* 2008; 53: 25–35.
  52. Uno K, Kumagai K, Khrestian CM, et al. New insights regarding the atrial flutter reentrant circuit: studies in the canine sterile pericarditis model. *Circulation* 1999; 100: 1354–1360.
  53. Ryu K, Shroff SC, Sahadevan J, et al. Mapping of atrial activation during sustained atrial fibrillation in dogs with rapid ventricular pacing induced heart failure: evidence for a role of driver regions. *J Cardiovasc Electrophysiol* 2005; 16: 1348–1358.
  54. Vigmond EJ, Tsoi V, Kuo S, et al. The effect of vagally induced dispersion of action potential duration on atrial arrhythmogenesis. *Heart Rhythm* 2004; 1: 334–344.
  55. Borek B, Shajahan TK, Gabriels J, et al. Pacemaker interactions induce reentrant wave dynamics in engineered cardiac culture. *Chaos* 2012; 22: 033132.
  56. Zhang H, Liu JH, Garratt CJ et al. Competitive interactions between ectopic foci and reentry in virtual human atrium. *Computers in cardiology* 2005; 32: 73–76.
  57. Gong Y, Xie F, Stein KM, et al. Mechanism underlying initiation of paroxysmal atrial flutter/atrial fibrillation by ectopic foci: a simulation study. *Circulation* 2007; 115: 2094–2102.
  58. Konings KT, Smeets JL, Penn OC, et al. Configuration of unipolar atrial electrograms during electrically induced atrial fibrillation in humans. *Circulation* 1997; 95: 1231–1241.
  59. Ryu K, Sahadevan J, Khrestian CM, et al. Use of fast fourier transform analysis of atrial electrograms for rapid characterization of atrial activation-implications for delineating possible mechanisms of atrial tachyarrhythmias. *J Cardiovasc Electrophysiol* 2006; 17: 198–206.
  60. Skanes AC, Mandapati R, Berenfeld O, et al. Spatiotemporal periodicity during atrial fibrillation in the isolated sheep heart. *Circulation* 1998; 98: 1236–1248.

61. Haissaguerre M, Sanders P, Hocini M, et al. Pulmonary veins in the substrate for atrial fibrillation: the “venous wave” hypothesis. *J Am Coll Cardiol* 2004; 43: 2290–2292.
62. Lin LJ, Billette J, Khalife K, et al. Characteristics, circuit, mechanism, and ablation of reentry in the rabbit atrioventricular node. *J Cardiovasc Electrophysiol* 1999; 10: 954–964.

#### **Author biographies**

**Catalina Tobón** is a full professor at the Universidad de Medellín, Department of Basic Science, Medellín, Colombia. She is part of the MATBIOM research group.

Her research interest is computer simulation in cardiovascular system.

**Javier Saiz** is a full professor at the Universitat Politècnica de València, Department of Electronic Engineering, Valencia, Spain and Director of the Center for Research and Innovation in Bioengineering and Coordinator of the MicroCluster on research in Personalized Medicine at the University. He has focused on the development of models for simulating cardiac arrhythmias and their different therapies.